



Defects and high bulk resistivities in the Bi-rich tetradymite topological insulator $\text{Bi}_{2+x}\text{Te}_{2-x}\text{Se}$

Shuang Jia,^{1,*} Haim Beidenkopf,² Ilya Drozdov,² M. K. Fuccillo,¹ Jungpil Seo,² Jun Xiong,² N. P. Ong,² Ali Yazdani,² and R. J. Cava¹

¹*Department of Chemistry, Princeton University, Princeton, New Jersey 08544, USA*

²*Department of Physics, Princeton University, Princeton, New Jersey 08544, USA*

(Received 8 August 2012; published 12 October 2012)

Defects in the topological insulator $\text{Bi}_2\text{Te}_2\text{Se}$ are studied by scanning tunneling microscopy. Small numbers of Te_{Bi} antisite defects are found and are postulated to be the origin of n -type carriers in this tetradymite composition near the n -to- p crossover. Based on this defect chemistry, we design an alternative method for obtaining resistive $\text{Bi}_{2+x}\text{Te}_{2-x}\text{Se}$ samples, by the introduction of compensating p -type carriers through Bi_{Te} antisite defects induced by making the material slightly Bi rich. Our resistivity and Hall coefficient measurements of $\text{Bi}_{2+x}\text{Te}_{2-x}\text{Se}$ crystals grown by the Bridgeman-Stockbarger method show that the carrier concentration at base temperature is significantly reduced from that of stoichiometric samples. Analysis of the measurements reveals the possible underlying chemical distribution along the boules during growth.

DOI: 10.1103/PhysRevB.86.165119

PACS number(s): 61.50.Ks, 74.25.Jb, 75.30.-m

I. INTRODUCTION

The discovery of spin-locked, gapless electronic states on the surfaces of three-dimensional (3D) topological insulators (TIs) has opened a new avenue for investigating electronic topological phenomena in condensed matter physics.^{1–5} Although surface-sensitive probes such as angle-resolved photoemission spectroscopy (ARPES) and scanning tunneling microscopy (STM) have been successfully employed for studying the exotic surface Dirac metallic state in TIs,^{6–12} the charge transport of the surface states has proven to be significantly more challenging to characterize. This is primarily because a very low concentration of defects in these narrow-band-gap semiconductors can easily induce high bulk conductivities that overwhelm conductivity from the surface states. Recently, attempts to make truly bulk insulating 3D TIs to allow characterization of surface transport have been focused on the tetradymite $(\text{Bi,Sb})_2(\text{Te,Se})_3$ family,^{13–19} archetypical thermoelectric materials that have been studied for more than 40 years.²⁰ It has been found that bulk crystals with resistivities higher than $1 \text{ } \Omega\text{cm}$ at low temperatures can be achieved by tuning the chemical composition of the tetradymites, leading so far to a best case in which the surface electrons contribute up to $\sim 50\%$ of the total conductance.^{18,19,21–23}

Among the tetradymite $(\text{Bi,Sb})_2(\text{Te,Se})_3$ family, the fully crystallographically ordered compound $\text{Bi}_2\text{Te}_2\text{Se}$ (BTS) has been the subject of significant crystal growth efforts relevant to its TI properties.^{21,22,24,25} Unlike the heavily doped parent compounds, p -type Bi_2Te_3 and n -type Bi_2Se_3 , BTS is located at the border of an n - p transition point while still keeping its full crystallographic order; the Se occupies the inner layer of the five-layer sandwich, while the Te occupies the outer layers.²⁶ Previous studies reported that carefully prepared BTS crystals manifest clear Shubnikov–de Hass oscillations of the surface states^{22,24} due to the high mobility of the surface electrons. However, most stoichiometric BTS crystals prepared by the modified Bridgman method are metallic conductors, with n -type carrier concentrations of the order of $\sim 10^{19}/\text{cm}^3$.²⁵ As previously reported, more highly resistive crystals can be prepared by either fine-tuning the selenium

composition or doping tin at the bismuth site,^{25,27} in order to introduce p -type carriers to compensate the n -type defects. Due to the complicated defect equilibria in this ternary compound, sample properties show a strong dependence on the initial chemical composition and large sample-to-sample variation within a single-crystal growth run.²⁵

Considering these difficulties in the reproducible preparation of resistive crystals, we were motivated to identify the defects in BTS crystals by a microscopic method. To perform this work, we selected a resistive BTS sample obtained by the modified Bridgman growth method from a stoichiometric initial composition and employed STM analysis to understand its defect equilibria. We show that the primary defects in this crystal are electronically neutral Se-Te antisite defects. In addition, a small number of Te_{Bi} antisite defects are observed, which produce n -type carriers. Calculations have shown that both of these types of defects are energetically favored in BTS.²⁸ Based on this result, we designed an alternative method for obtaining resistive $\text{Bi}_{2+x}\text{Te}_{2-x}\text{Se}$ crystals by introducing compensating p -type carriers through the introduction of small amounts of Bi substitution for Te expected to form Bi_{Te} antisite defects. Our resistivity and Hall coefficient measurements on $\text{Bi}_{2+x}\text{Te}_{2-x}\text{Se}$ samples made by the Bridgeman-Stockbarger method show, for $0.015 < x < 0.06$, that these crystals display a significantly reduced carrier concentration at low temperatures. For $x \geq 0.02$, parts of the 14-cm-long boules start to show a high resistivity and low carrier concentrations, while almost the whole boule becomes resistive, with a p -type carrier concentration, at low temperatures when $x = 0.06$. Thus we report that Bi excess BTS crystals can be grown reliably with high bulk resistivities and are, therefore, good candidates for the study of surface currents in 3D TIs.

II. EXPERIMENT AND RESULTS

A. Observation of effects

Our previous investigations of BTS crystals grown by the modified Bridgeman method yielded a few batches of resistive BTS samples from a stoichiometric nominal starting composition.²² Realizing the strong sample dependence of

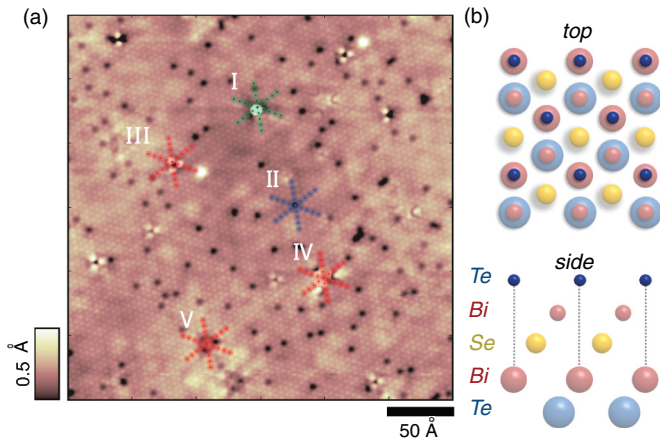


FIG. 1. (Color online) (a) Topographic image ($V_{\text{bias}} = 500$ mV, $I = 30$ pA) of the surface of BTS showing five types of defects. (b) Schematic structure of a quintuple layer in BTS. The cleavage plane lies between two Te layers in adjacent quintuple-layer sandwiches. Upon looking into the basal plane, the first inner layer that registers with the upper Te layer is the layer of Bi three layers deeper (registry shown by the dotted line).

properties even in nominally equivalent crystal growths, we selected crystals for STM characterization from a batch with resistivities higher than $1 \Omega\text{cm}$, with n -type behavior at 4 K. Crystals were cleaved *in situ* and measured under UHV at 4 K in a home-built STM.

The topographic image in Fig. 1(a) shows atomic corrugations on the sample surface of BTS. Since the Te-Bi-Se-Bi-Te quintuple-layer sandwich is strongly bonded internally²⁶ [see top and side views in Fig. 1(b)], the cleavage is at the van der Waals bonds between sandwiches, and thus the imaged atoms on the exposed surface are Te atoms. In the image, we find five types of defects. We classify them by their registry with the lattice and their lateral size: the larger the imaged defect is laterally, the deeper it resides below the surface.²⁹ Defect I appears as an ~ 1 -Å-high circular hump; these we identify as adatoms remnant from the cleavage process. There is a very small number of them in this image, which shows about 10 000 surface layer atom sites. Defect II registers with a single lattice site and thus is embedded in the upper Te layer. This defect appears as a dip in both occupied and empty state topographies, therefore signifying that it is electrically neutral. It is the most abundant defect observed, occupying $\sim 2.5\%$ of the imaged lattice; this defect is absent in the binary compounds Bi_2Te_3 and Bi_2Se_3 . These features strongly suggest that defect II is a Se-Te antisite defect. The fact that there are two equivalent Te layers per quintuple-layer sandwich doubles its abundance in the crystal to $\sim 5\%$, which is in agreement with our previous structural determination of BTS.²⁵ The dominance of these neutral Se_{Te} defects is consistent with calculations.²⁸ Defect III is triangular, with an edge length of two atoms, centered directly between lattice sites in the upper Te layer. It thus resides in the Bi layer just below the upper Te layer. This defect is identified as either a Te or a Se antisite defect on the Bi layer; the Te_{Bi} antisite is energetically preferred.²⁸ These defects act as charge donors and therefore render the crystal n -type. Finally, defects IV and V are both large and register with the upper Te lattice, suggesting that they are Te or Se

antisite defects located in the deeper Bi layer [see Fig. 1(b)]; these defects thus dope the crystal with electrons, like defect III does. Interestingly, we find no traces of the defects that are common in the parent binary compounds—vacancies in Bi_2Se_3 (which would register with the lattice and extend over three sites) or Bi substitution for Te antisite defects (which would appear as charged defects in the upper Te layers), the dominant defects rendering the parent binaries n - and p -type, respectively.^{13,20,30} The dominant charged dopants that we have observed in native BTS are therefore Bi_{Te} antisite defects. These defects render the crystals n -type and shift the chemical potential to be above the surface Dirac point in the bulk gap.

In order to better characterize the exact doping level of these highly resistive samples with respect to the surface-state dispersion curve, we imaged the dispersive interference pattern that the surface Dirac electrons form in the vicinity of crystallographic defects. The topographic image in Fig. 2(a) shows a nanoscale crack on the surface of BTS; differential conductance (dI/dV) line scans were measured along the dotted arrow. The resulting oscillating local density of states is shown in Fig. 2(b), where the second derivative d^2I/dV^2 was taken numerically to suppress the dc background. As a result, we were able to resolve a standing wave pattern at almost all energies. The wavelength increases as the bias is lowered. While the oscillating pattern at high energies decays rather rapidly, at lower energies the pattern remains remarkably coherent throughout our field of view. This unusual robustness may very well have to do with the topological protection against backscattering of the Dirac surface states within the bulk gap.

To further study the dispersion of the interference pattern, we calculated its Fourier transform, which is shown in Fig. 2(c). The pattern shows that we clearly resolve a linearly dispersing scattering mode (dotted line) persisting almost down to the zero momentum transfer that signifies the Dirac energy. The Fermi velocity for this mode is consistent with what is seen in the ARPES spectra for BTS.^{31,32}

Linear extrapolation of this mode sets the Dirac-point energy at 300 meV below the Fermi energy, confirming the n -type nature of these resistive BTS samples. Nevertheless, the phase space between the linearly dispersing modes for scattering from the crack seems to get occupied above ~ 70 meV; we associate this with the onset of the bulk conduction band above that energy. This yields a bulk gap of ~ 370 meV, in agreement with the values measured in ARPES for BTS.^{31,32} More importantly, this sets the chemical potential for these crystals within the bulk gap, a very important requirement for the observation of surface transport in 3D TIs. The features inside the Dirac cone in Fig. 2(c) are due to noise in the interference pattern.

A potential problem that defects might introduce on the surface of a TI is a spatially varying chemical potential (as well as a spatially varying Dirac-point energy).³³ This would result if the defects are electrically charged. To test whether this happens in BTS, we performed extensive differential conductance line scans, as demonstrated in Fig. 3. Topographically, the neutral 2.5% Te-Se antisite defects on the cleavage surface layer in BTS make the surface appear highly disordered, even more so than the surface of 2.5% Mn-doped Bi_2Se_3 [insets in Figs. 3(a) and 3(b), respectively]. Nevertheless, the differential

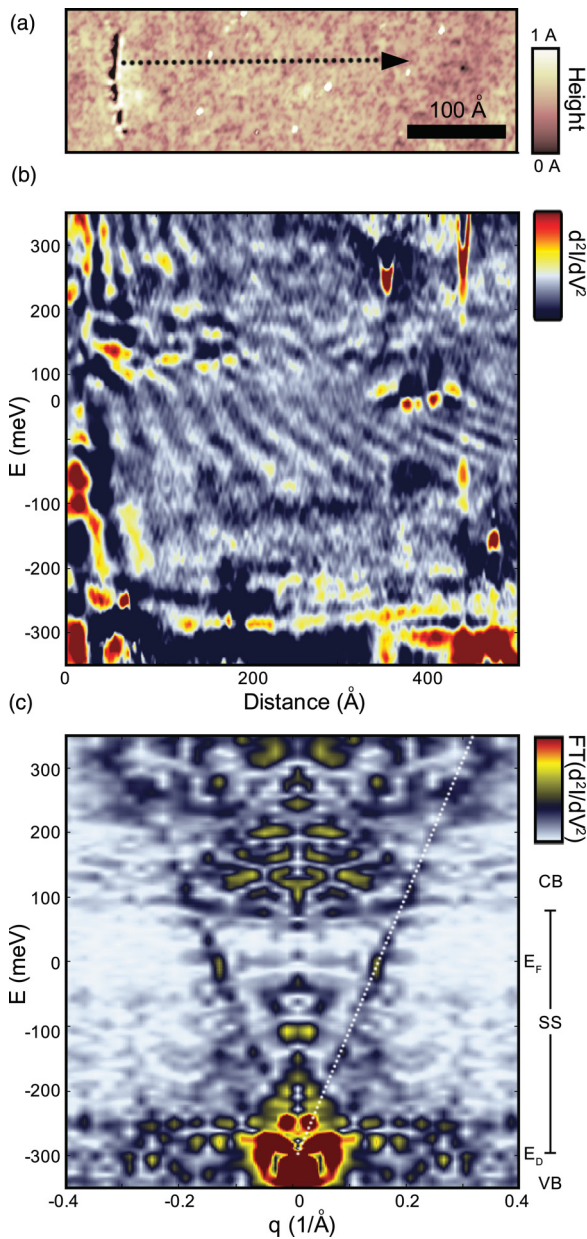


FIG. 2. (Color online) (a) Topographic images of a 50-Å-long crack on the surface of BTS. A dI/dV line scan was taken along the dotted arrow. (b) To eliminate background, a second derivative $d(dI/dV)/dV$ was taken numerically. This line scan reveals a dispersing standing wave pattern in the local density of states. (c) Its Fourier transform shows a linearly dispersing scattering mode (marked by the dotted line) that extrapolates to 300 meV below the Fermi energy.

conductance measurements across these surfaces reveal that the chemical potential does not vary substantially in BTS (with a standard deviation of ~ 2 meV. In contrast, Mn dopants on the Bi sites in Bi_2Se_3 are charged (as are other charged native defects) and make the local density of states shift as a whole from point to point on the surface due to underlying electrostatic potential variations. These variations are more than 30 meV. Thus an unanticipated positive characteristic of BTS is that the defects present do not significantly disturb the chemical potential at the surface, making the surface hosting

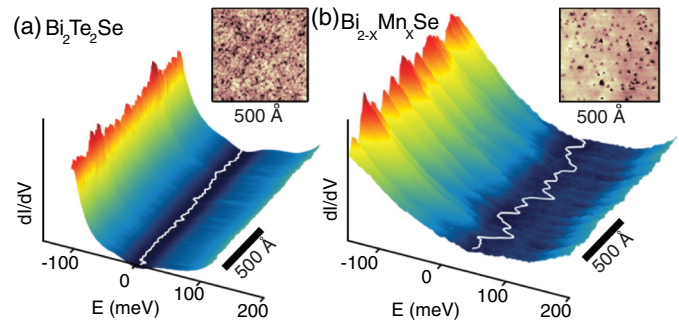


FIG. 3. (Color online) (a) An extended dI/dV line scan over the highly defective surface (the inset shows its topography) of a BTS crystal shows only minor fluctuations of the spectrum because the majority of the defects are neutral. (b) For comparison, a similar line scan taken on the surface of 2.5% Mn-doped Bi_2Se_3 exhibits large energy fluctuations of the measured dI/dV spectrum due to charged substitutional Mn.

the topological surface states more electrically uniform on the nanometer length scale.

B. Characterization of transport

Our STM investigation revealed that resistive n -type BTS samples show no observable Se vacancies, while Te_{Bi} antisite defects are the main defects introducing n -type carriers. Such highly resistive BTS samples were not, however, obtained reliably through the modified Bridgman or the Bridgeman-Stockbarger methods from nominally stoichiometric melts; most of these samples showed heavily doped n -type metallic behavior.²⁵ The Te_{Bi} antisite defects identified by STM motivated us to seek more reliably high-resistivity samples by investigating a controllable p -type doping parameter: the Bi_{Te} antisite defects introduced by intentionally adding extra Bi in small amounts to the initial composition. We therefore grew a series of $\text{Bi}_{2+x}\text{Te}_{2-x}\text{Se}$ crystals, with a maximum x of 0.06, by the classic Bridgeman-Stockbarger method.^{25,34} The boules obtained in these growths are approximately 14 cm in length and 0.6 cm in diameter. Due to the chemical composition distribution that naturally occurs along crystal boules during such growth, the electrical properties at different positions in the boules are expected to be different. Therefore the boules were cut to seven pieces of about 2-cm length for individual investigation. The parts of each boule are labeled from A, the ending point of the crystal growth, to G, the starting point of the growth. Bar-shaped samples with a typical thickness of 0.1 to 0.02 mm, cleaved along the basal plane, were selected for the resistivity and Hall measurements, which were performed by a standard four-point or five-point method in a Quantum Design Physical Property Measurement System (PPMS) from 300 to 10 K. Considering the samples' expected variation in defect concentration, we selected multiple pieces from each region for measurements; only representative results are presented in this report.

Figure 4 shows the temperature-dependent in-plane single-crystal resistivities, as $R/R_{300\text{K}}$, for $\text{Bi}_{2+x}\text{Te}_{2-x}\text{Se}$ for representative $x = 0, 0.015, 0.02,$ and 0.04 crystals. Almost all parts of the boule show metallic behavior for $x \leq 0.01$. For $x \geq 0.015$, the crystals cut from the middles of the

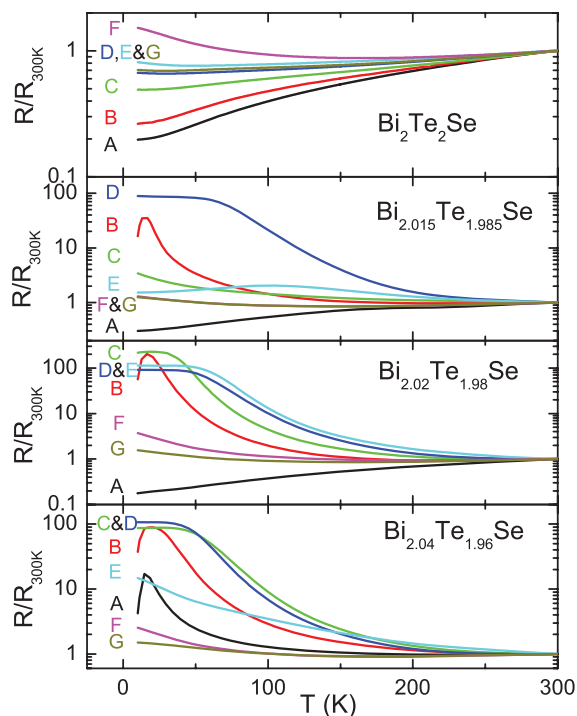


FIG. 4. (Color online) Normalized in-plane temperature-dependent resistivities for $\text{Bi}_{2+x}\text{Te}_{2-x}\text{Se}$ crystals for $x = 0, 0.015, 0.02,$ and 0.04 . Labels A to G represent samples selected from 2-cm sections, from the ending (A) to the starting (G) points of the growth of the boule.

boules (parts B–E) show resistivities that increase rapidly with decreasing temperature below 100 K. Highly resistive samples ($R_{10\text{K}}/R_{300\text{K}} > 100$) are found in the middles of the boules for $x \geq 0.02$. When $x \geq 0.04$, all parts of the boules show $R_{10\text{K}}/R_{300\text{K}} > 1$. It is worth noting that while most of the insulating samples show a resistivity that saturates at low temperatures, some samples show resistivity drops below 25 K (e.g., sample B for $x = 0.015$ and 0.02). Those samples also show resistivities that rise with decreasing T at a relatively lower temperature than is seen for other resistive samples. This behavior is correlated with changes in carrier concentration, as described below.

Figure 5 shows the temperature-dependent Hall coefficients (R_H) for $\text{Bi}_{2+x}\text{Te}_{2-x}\text{Se}$ for a range of x values. For $x = 0.0$, all of the samples show small negative R_H values, indicative of relatively high electron carrier concentrations, consistent with their low resistivities. For $x \geq 0.015$, most of the highly resistive samples in the middles of the boules show similar temperature-dependent changes in R_H : R_H initially increases with decreasing T , leading to a positive maximum below 100 K; it then decreases with further decreasing T , crosses 0, and shows a negative maximum at low temperatures. This behavior is similar to previous observations.^{21,22,24,25} Consistent with this behavior, the resistivities of these samples rise to a high value below 100 K and then saturate at low temperatures. For samples showing anomalous resistivity drops at low temperatures, R_H shows a positive maximum at relatively lower temperatures (e.g., sample B for $x = 0.015$ and 0.02). A few samples (e.g., sample C for $x = 0.02$ and 0.04) show positive carrier contributions at low temperatures,

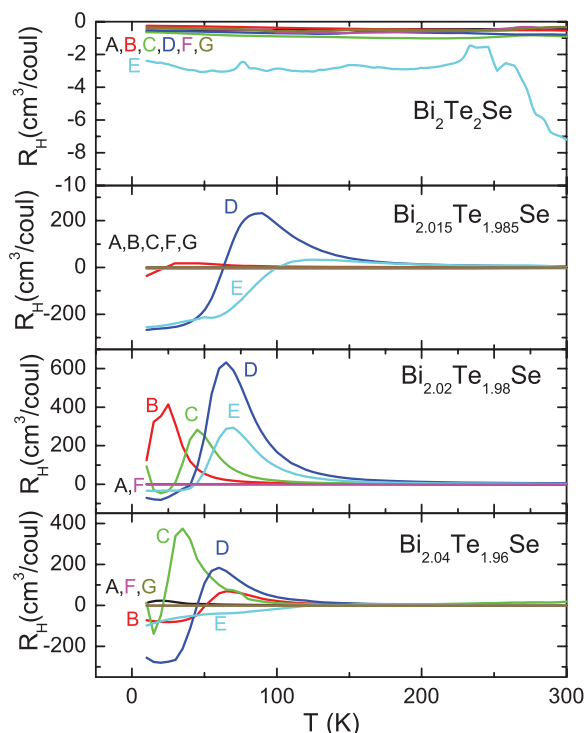


FIG. 5. (Color online) Temperature-dependent Hall coefficient for $\text{Bi}_{2+x}\text{Te}_{2-x}\text{Se}$ for $x = 0, 0.015, 0.02,$ and 0.04 crystals. Samples are the same ones used to measure $R(T)$ in Fig. 4 and are similarly labeled A through G.

leading R_H to cross 0 to a small positive value. The origin of the anomalous behavior of these samples is not yet clear, but we believe that it is correlated with the contribution from the bulk valence band when the Fermi level (E_F) is very close to the top of the valence band. It is tempting to attribute the observed saturation of or decrease in the resistivity at low temperatures in the resistive samples (Fig. 4) to a short-circuiting effect of the surface-state currents. However, the corresponding changes in bulk carrier concentrations (Fig. 5) indicate that this phenomenon, rather, occurs in the bulk of the crystals, likely reflecting a temperature dependence of the details of the bulk band structure.

In order to characterize the variations in properties with position along the crystal boules, the resistivities and carrier concentrations at 10 K ($\rho_{10\text{K}}$ and n or p), for different parts of the boules at representative x values, are plotted in Figs. 6(a) and 6(b), respectively. The starting ($l = 12$ cm) and ending ($l = 0$ cm) points of the crystal growth always show relatively low $\rho_{10\text{K}}$ values, with higher resistivity samples found in the middle region (between 4 and 6 cm). At a higher x , the whole boule becomes more resistive, and about 4 cm of the boule shows $\rho_{10\text{K}} > 1 \Omega\text{cm}$ for $x \geq 0.02$. About 10 cm of the boule displays $\rho_{10\text{K}} > 1 \Omega\text{cm}$ for $x = 0.06$. We assume for the sake of discussion that a single band dominates the carrier contributions at the base temperature. The carrier concentrations thus determined from the Hall coefficient data at 10 K are shown in Fig. 6(b), as a function of the position along the boule. [This simplified model may not explain the behavior of the samples showing additional p -type contributions at low temperatures (i.e., sample C for $x = 0.04$).] As shown in Fig. 6(b), the whole

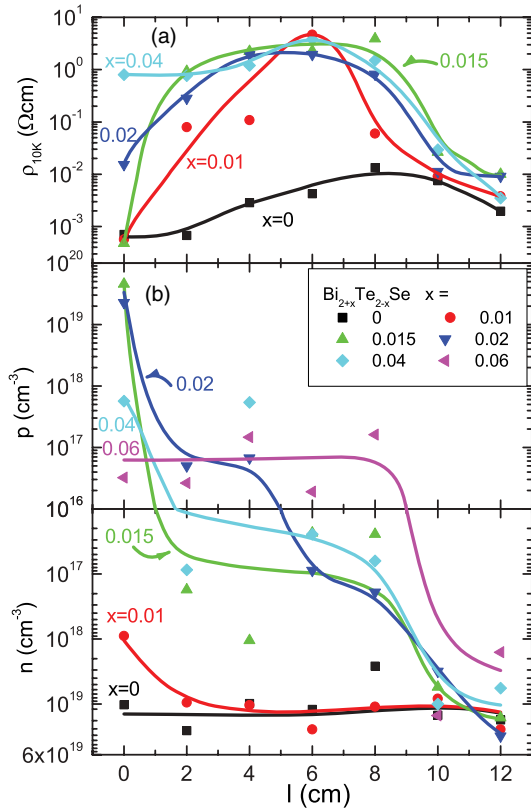


FIG. 6. (Color online) (a) Resistivities at 10 K of $\text{Bi}_{2+x}\text{Te}_{2-x}\text{Se}$ for $x = 0, 0.015, 0.02, 0.04,$ and 0.06 for different positions in the crystal growth boule (0 marks the last-to-crystallize end of the crystal). (b) In-plane Hall coefficients at 10 K. The sample at $l = 4$ cm (sample C) for $x = 0.04$, which deviates most from the general trend, has anomalous p -type carriers occurring at the lowest temperature measured. The lines are guides for the eye.

boule is heavily doped n -type for $x \leq 0.01$. The later sections of the boule become p -type for $x \geq 0.015$, while the part that is the first to crystallize remains heavily doped n -type ($n \sim 2 \times 10^{19}/\text{cm}^3$ to $1 \times 10^{18}/\text{cm}^3$) for all samples. This variation leads to an n -to- p transition along the boule, yielding low-carrier-concentration (n - or p -type) samples in the middle. Additional Bi makes the whole boule more p -type, and all but the last-to-crystallize part of the $x = 0.06$ boule are p -type. The points that fall farthest from the general trend (i.e., at $l = 4$ cm for $x = 0.04$) are from the crystals that show anomalous positive R_H contributions at the lowest temperatures measured.

III. DISCUSSION AND CONCLUSION

In order to obtain highly resistive bulk samples of BTS-based TIs, previously reported crystal growth studies compensated the native n -type carriers present by means of employing external elements, i.e., Sn doping at the Bi site for BTS,²⁷ high quantities of Sb substitution for Bi,^{18,19} and Ca doping at the Bi site for Bi_2Te_3 .¹³ The defect equilibria for Sn^{2+} and Ca^{2+} doping at the Bi site has shown those defects to be effective charge +1 acceptors with low ionization energies at low doping levels; they appear to contribute p -type carriers in proportion to their doping level.^{13,27} For Bi_2Te_3 , Bi_{Te} antisite defects act as effective 1^+ acceptors that are fully ionized at

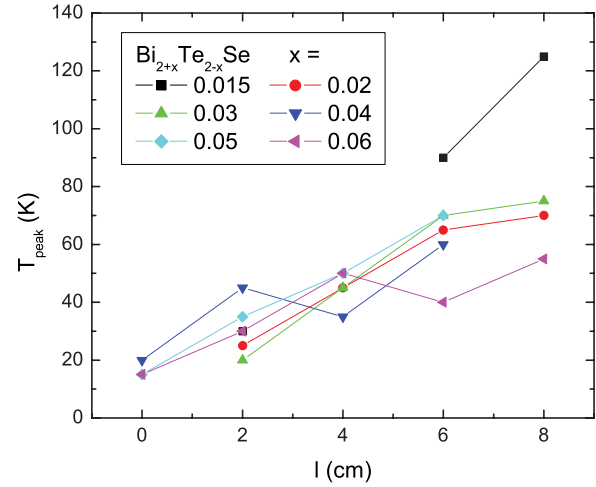
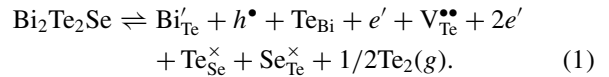
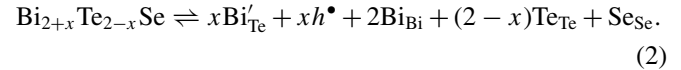


FIG. 7. (Color online) The temperature at which R_H shows a positive maximum value for $0.015 \leq x \leq 0.06$ as a function of position in the boule. 0 marks the last-to-crystallize end of the crystal.

100 K.²⁰ In accordance with theoretical calculations²⁸ and the current experimental study, we postulate the following defect chemistry for native BTS:



In the presence of excess Bi, which compensates for the two sources of electrons, the excess Bi_{Te} antisite defects in $\text{Bi}_{2+x}\text{Te}_{2-x}\text{Se}$ are acceptors, with the defect equilibrium:



The total number of excess holes created by the Bi_{Te} antisite defects, however, appears to be much lower than the number of antisite defects present. As shown in Fig. 7, for example, only the last-to-crystallize part of the boule (sample A) for $x = 0.015$ manifests $p = 5 \times 10^{19}/\text{cm}^3$ at 10 K, which is lower than the concentration of the Bi_{Te} antisite defects present, calculated from the chemical formula as ($\sim 10^{20}/\text{cm}^3$). When x increases, the p -type carrier concentration decreases at 10 K. The samples for $x = 0.06$ in $\text{Bi}_{2+x}\text{Te}_{2-x}\text{Se}$ are highly resistive, with $p \sim 10^{17}/\text{cm}^3$, at 10 K. For comparison, $\text{Bi}_{2+x}\text{Te}_{3-x}$ shows strongly metallic behavior, with $p \sim 2 \times 10^{20}/\text{cm}^3$, at 100 K.²⁰ All the p -type samples for $0.015 \leq x \leq 0.06$ show p of the order of $10^{19}/\text{cm}^3$ at room temperature (not shown in the plots), which is one or two orders of magnitude less than expected from the chemical doping level.

The changes in the p -type carrier concentration and resistivity suggest that there may be more complicated defect equilibria and excitation energetics at high Bi_{Te} antisite defect concentrations. One possibility is that the Bi_{Te} antisite defects may form an impurity band at high concentrations. If this impurity band is located in the bulk band gap, then it may pin E_F in the bulk band gap and induce a higher resistivity. On the other hand, of course, the likely complexity of the Fermi surface in bulk BTS should also preclude a simple 1:1 correspondence of chemical and electronic doping. Detailed characterization of the Fermi surface of bulk BTS near the n -to- p crossover has never been performed, to our knowledge; further investigations

beyond the current transport measurements would therefore be of interest. Quantitative interpretation of the correlations between chemical and electronic doping depends on detailed models, beyond the scope of this study, which include, for example, the effects of Fermi level pinning.²⁸

During the BTS crystal growth by the Bridgman-Stockbarger method, there are two factors expected to affect the chemical distribution along the boule. First, the temperature gradient induces a distribution of the chemical composition in the solid solution, which can be assumed to have a small stoichiometry-dependent variation in melting point.³⁵ This is likely to be one major influence on the variation of electronic properties along the boule. In addition, due to the relative stability of vacant Te sites and the vapor pressure of tellurium, the 14-cm-long vertical melt is expected to crystallize under a higher Te vapor pressure at the top (which becomes the end point of the boule upon solidification) than the bottom (the starting point of the boule upon crystallization). Thus a subtle Te distribution gradient may also contribute to the charge carrier distribution on the boules; with a larger Te deficiency at the starting point of crystallization the samples will tend to be *n*-type, while at the middles and end points of the boules Te deficiency must be at a low level, since Te vacancies are not detectable by STM. Therefore these regions may be more responsive to *p*-type doping through the excess Bi. Finally, of course, due to the directional solidification of the boule, randomly present impurity atoms are expected to concentrate in the last-to-crystallize portion, influencing its carrier concentration.

Consideration of the temperature-dependent R_H is consistent with these subtle chemical distribution effects along the boule. As shown in Fig. 7, the temperature of the positive maximum in R_H (i.e., the T_{peak}) decreases with position along the crystal growth direction in the boule for all resistive samples. Our previous report on the behavior of nearly stoichiometric BTS crystals under pressure revealed that a satellite hole pocket lower than the chemical potential²³ contributed the *p*-type carriers at high temperatures. The temperature-dependent R_H for $\text{Bi}_{2+x}\text{Te}_{2-x}\text{Se}$ is similar to that for the nearly stoichiometric BTS samples, while the change in the T_{peak} along the boule may be a reflection of the shift of the chemical potential along the boule, from the bottom of the conduction band to the top of the valence band. This analysis is consistent with our assumption of the presence of small Te and Bi concentration gradients along the boule, although a more complicated defect effect is anticipated for the higher Bi_{Te} antisite-defect-containing samples in this study. A comparative study of the defects in Bi-rich and Bi-poor samples of BTS by STM would be of future interest.

ACKNOWLEDGMENTS

The authors are thankful for helpful discussions with J. Allred, Huiwen Ji, and M. E. Charles. The crystal growth and STM characterization were supported by SPAWAR Grant No. N6601-11-1-4110 and by the NSF MRSEC program through Grant No. DMR-0819860. The defect chemistry work was supported by AFOSR Grant No. FA9550-10-1-0533.

*Corresponding author: jia@princeton.edu

¹L. Fu and C. L. Kane, *Phys. Rev. B* **76**, 045302 (2007).

²L. Fu, C. L. Kane, and E. J. Mele, *Phys. Rev. Lett.* **98**, 106803 (2007).

³J. E. Moore and L. Balents, *Phys. Rev. B* **75**, 121306 (2007).

⁴M. Z. Hasan and C. L. Kane, *Rev. Mod. Phys.* **82**, 3045 (2010).

⁵X.-L. Qi and S.-C. Zhang, *Rev. Mod. Phys.* **83**, 1057 (2011).

⁶D. Hsieh, Y. Xia, D. Qian, L. Wray, F. Meier, J. H. Dil, J. Osterwalder, L. Patthey, A. V. Fedorov, H. Lin *et al.*, *Phys. Rev. Lett.* **103**, 146401 (2009).

⁷Y. Xia, D. Qian, D. Hsieh, L. Wray, A. Pal, H. Lin, A. Bansil, D. Grauer, Y. S. Hor, R. J. Cava *et al.*, *Nat. Phys.* **5**, 398 (2009).

⁸Y. L. Chen, J. G. Analytis, J.-H. Chu, Z. K. Liu, S.-K. Mo, X. L. Qi, H. J. Zhang, D. H. Lu, X. Dai, Z. Fang *et al.*, *Science* **325**, 178 (2009).

⁹Y. L. Chen, Z. K. Liu, J. G. Analytis, J.-H. Chu, H. J. Zhang, B. H. Yan, S.-K. Mo, R. G. Moore, D. H. Lu, I. R. Fisher *et al.*, *Phys. Rev. Lett.* **105**, 266401 (2010).

¹⁰T. Sato, K. Segawa, H. Guo, K. Sugawara, S. Souma, T. Takahashi, and Y. Ando, *Phys. Rev. Lett.* **105**, 136802 (2010).

¹¹S.-Y. Xu, Y. Xia, L. A. Wray, S. Jia, F. Meier, J. H. Dil, J. Osterwalder, B. Slomski, A. Bansil, H. Lin *et al.*, *Science* **332**, 560 (2011).

¹²P. Cheng, C. Song, T. Zhang, Y. Zhang, Y. Wang, J.-F. Jia, J. Wang, Y. Wang, B.-F. Zhu, X. Chen *et al.*, *Phys. Rev. Lett.* **105**, 076801 (2010).

¹³Y. S. Hor, A. Richardella, P. Roushan, Y. Xia, J. G. Checkelsky, A. Yazdani, M. Z. Hasan, N. P. Ong, and R. J. Cava, *Phys. Rev. B* **79**, 195208 (2009).

¹⁴J. G. Checkelsky, Y. S. Hor, M.-H. Liu, D.-X. Qu, R. J. Cava, and N. P. Ong, *Phys. Rev. Lett.* **103**, 246601 (2009).

¹⁵D.-X. Qu, Y. S. Hor, J. Xiong, R. J. Cava, and N. P. Ong, *Science* **329**, 821 (2010).

¹⁶J. G. Analytis, R. D. McDonald, S. C. Riggs, J.-H. Chu, G. S. Boebinger, and I. R. Fisher, *Nat. Phys.* **6**, 960 (2010).

¹⁷N. P. Butch, K. Kirshenbaum, P. Syers, A. B. Sushkov, G. S. Jenkins, H. D. Drew, and J. Paglione, *Phys. Rev. B* **81**, 241301 (2010).

¹⁸Z. Ren, A. A. Taskin, S. Sasaki, K. Segawa, and Y. Ando, *Phys. Rev. B* **84**, 165311 (2011).

¹⁹A. A. Taskin, Z. Ren, S. Sasaki, K. Segawa, and Y. Ando, *Phys. Rev. Lett.* **107**, 016801 (2011).

²⁰D. M. Rowe, *Handbook of Thermoelectrics*, 6th ed. (CRC Press, Boca Raton, FL, 1995).

²¹J. Xiong, Y. Luo, Y. H. Khoo, S. Jia, R. J. Cava, and N. P. Ong, *Phys. Rev. B* **86**, 045314 (2012).

²²J. Xiong, A. C. Petersen, D. Qu, R. J. Cava, and N. P. Ong, *Physica E* **44**, 917 (2012).

²³Y. Luo, S. Rowley, J. Xiong, S. Jia, R. J. Cava, and N. P. Ong, arXiv:1110.1081.

²⁴Z. Ren, A. A. Taskin, S. Sasaki, K. Segawa, and Y. Ando, *Phys. Rev. B* **82**, 241306 (2010).

- ²⁵S. Jia, H. Ji, E. Climent-Pascual, M. K. Fuccillo, M. E. Charles, J. Xiong, N. P. Ong, and R. J. Cava, *Phys. Rev. B* **84**, 235206 (2011).
- ²⁶S. Nakajima, *J. Phys. Chem. Solids* **24**, 479 (1963).
- ²⁷Z. Ren, A. A. Taskin, S. Sasaki, K. Segawa, and Y. Ando, *Phys. Rev. B* **85**, 155301 (2012).
- ²⁸D. O. Scanlon, P. D. C. King, R. P. Singh, A. de la Torre, S. M. Walker, G. Balakrishnan, F. Baumberger, and C. R. A. Catlow, *Adv. Mater.* **24**, 2154 (2012).
- ²⁹S. Urazhdin, D. Bilc, S. H. Tessmer, S. D. Mahanti, T. Kyratsi, and M. G. Kanatzidis, *Phys. Rev. B* **66**, 161306 (2002).
- ³⁰G. Wang, X.-G. Zhu, Y.-Y. Sun, Y.-Y. Li, T. Zhang, J. Wen, X. Chen, K. He, L.-L. Wang, X.-C. Ma *et al.*, *Adv. Mater.* **23**, 2929 (2011).
- ³¹M. Neupane, S.-Y. Xu, L. A. Wray, A. Petersen, R. Shankar, N. Alidoust, C. Liu, A. Fedorov, H. Ji, J. M. Allred *et al.*, *Phys. Rev. B* **85**, 235406 (2012).
- ³²T. Arakane, T. Sato, S. Souma, K. Kosaka, K. Nakayama, M. Komatsu, T. Takahashi, Z. Ren, K. Segawa, and Y. Ando, *Nat. Commun.* **3**, 636 (2012).
- ³³H. Beidenkopf, P. Roushan, J. Seo, L. Gorman, I. Drozdov, Y. S. Hor, R. J. Cava, and A. Yazdani, *Nat. Phys.* **7**, 939 (2011).
- ³⁴A. Hruban, A. Materna, W. Dalecki, G. Strzelecka, M. Piersa, E. Jurkiewicz-Wegner, R. Diduszko, M. Romaniec, and W. Orłowski, *Acta Phys. Pol. A* **120**, 950 (2011).
- ³⁵W. G. Pfann, *Zone Melting, Wiley Series Sci. Tech. Mat.*, 2nd ed. (Wiley, New York, 1966).